Quantifying the relation between the morphology and performance of polymer solar cells using Monte Carlo simulations

Bao Lei, Yan Yao, Ankit Kumar, Yang Yang,[a] and Vidvuds Ozolins[b]
Department of Materials Science and Engineering, University of California, Los Angeles, Los Angeles, California 90095-1595, USA

(Received 18 July 2007; accepted 13 May 2008; published online 21 July 2008)

Morphology is a crucially important factor determining the efficiency of photocurrent generation in bulk heterojunction polymer solar cells. Morphology, which depends on the characteristics of the polymers as well as on the conditions of phase separation, affects the performance of solar cells by influencing the rate of exciton dissociation and the efficiency of charge carrier transport. Using Monte Carlo simulations, we investigate the effects of annealing time on the morphology of phase separation and charge transfer behavior inside the active layers of polymer solar cells. We find that a suitably defined correlation distance is an effective parameter that quantitatively characterizes different morphologies and can be used to establish a direct link with transmission electron microscopy images of real polymer solar cells. Optimal morphologies have been investigated, showing results that are consistent with experimental data. © *2008 American Institute of Physics*. [DOI: 10.1063/1.2956689]

I. INTRODUCTION

The recent surge of interest in the science and technology of solar cells can be attributed to a growing shortage of fossil fuels, as well as to a need for environmentally friendly clean sources of energy.[1] Polymer photovoltaics are particularly attractive because of their ease of fabrication, flexibility, low weight, and low cost.[2,3] Polymer solar cells with demonstrated efficiencies of more than 5% are considered to be promising alternatives to their inorganic counterparts.[4–7]

Efficiency of polymer solar cells can be enhanced by the bulk heterojunction structure, which consists of blends of electron donor polymers and electron acceptor molecules.[8] The mechanism of photocurrent generation in these systems involves a sequence of steps starting with the generation of excitons by incident photons. Excitons are quasiparticles having short lifetimes of several hundreds of picoseconds[9] and diffusion lengths of about 10 nm.[10] The photogenerated excitons diffuse and, upon reaching the interface between the electron donor and electron acceptor materials, separate into electrons and holes. These charge carriers transfer inside the active layer, under a built-in electric field and/or external bias voltage, until they are extracted by the electrodes and contribute to the photocurrent.

The morphology of the two phases in the active layer is therefore of crucial importance for the performance of solar cells.[4,11–15] A morphology that maximizes the interfacial area between the materials will improve the dissociation rate of the excitons, leading to higher efficiencies.[16] On the other hand, too much interfacial area would increase the chances for the electron-hole recombination, as well as make the conduction path longer, which would lead to a decrease in efficiency.

Several models are available in the literature to treat this problem.[17,9,18] Sylvester-Hvid *et al.* developed a two-dimensional (2D) model, which was used to establish the morphology dependence of the short circuit current.[17] However, morphology inputs were just ideal 2D matrices and the possibility of network formation was not considered. The Monte Carlo simulations of Watkins *et al.*[9] covered the full sequence from morphology generation to electron transfer, and the results showed that the quantum efficiency is a function of the donor-acceptor interfacial area. However, the topic of quantitative characterization of the morphology and its relation to the photovoltaic performance remains largely unexplored.

In the present work, using Monte Carlo simulations of morphology generation and carrier transport, we correlate the annealing process in the fabrication stage with the photocurrent and use this relationship to evaluate different morphologies. We introduce the concept of correlation distance as a simple experimentally accessible way of characterizing two-phase morphologies, which allows us to describe the optimal morphology quantitatively.

II. MONTE CARLO MODELING OF POLYMER SOLAR CELLS

We use a 2D lattice system to model the solar cell device. The active layer of the solar cell is described as a 2D matrix with each element representing an *N*-type (acceptor) material or a *P*-type (donor) material at its position. The cathode and anode are modeled as two extra rows appended to the top and the bottom of the matrix.

A. Morphological evolution

The inherent properties of intermolecular interactions and conformational entropies of the electron donor and acceptor molecules in polymer blends are such that molecules of a given kind prefer to be surrounded by molecules of the same kind. Therefore, upon annealing, the system tends to

[a]Electronic mail: yangy@ucla.edu.
[b]Electronic mail: vidvuds@ucla.edu.

phase separate and decrease the degree of intermixing between the two phases; the degree of phase separation is commonly characterized by the total interfacial area between the two polymers.

Since the phase separation in polymer systems is usually a process driven by entropy (which is larger in the phase-separated state than in the mixed state), we calculate the total free energy, $F=E-TS$, as a product of temperature and entropy only, neglecting the energy term altogether. In our 2D model, each grid point on a simple square lattice stands for a site, which can be occupied either by an *N*- or a *P*-type molecule. The entropy and free energy associated with a site i are calculated using the nearest-neighbor Ising model expression:

$$S_i = J\sum_j^N s_i s_j,$$

$$F_i = -TS = -TJ\sum_j^N s_i s_j, \tag{1}$$

where J is the coupling constant and the discrete spinlike variables s_i and s_j denote the identities of phases for sites i and j, taking the values of +1 and −1 for the *N*- and *P*-type phases, respectively. Since molecules beyond the nearest neighbors will have a relatively small effect on the entropy of site i, their effect is not included in Eq. (1). Then the total free energy is calculated as

$$F_i = -TJ\sum_i \sum_{j\in NNi} s_i s_j. \tag{2}$$

A standard nearest-neighbor exchange Monte Carlo method (Kawasaki dynamics) is used to simulate the kinetics of phase separation. We start from a random distribution of the two phases on the lattice sites. At each Monte Carlo step, we randomly pick two nearest-neighbor sites, swap them, and calculate the change in the total free energy, ΔF. The acceptance probability depends on the change in the total free energy as

$$P(\Delta F) = \frac{1}{1+\exp\left(\frac{\Delta F}{k_B T}\right)}. \tag{3}$$

The main simplification of our model is the linear temperature dependence of the free energy in Eq. (2), which results in a temperature-independent Boltzmann weight in Eq. (3). This leads to computer-generated morphologies that depend only on the number of Monte Carlo steps. Temperature enters the kinetics of diffusion via the actual time represented by each Monte Carlo step. However, in real experiments, variations in the temperature will influence not only the diffusion rate but also the evaporation rate of solvent, crystallinity of the polymer, and many other factors that are difficult to treat within the simple Ising model. Future studies considering the solvent annealing and evaporation effects will give a more realistic temperature dependence of morphologies. Nevertheless, Eqs. (1)–(3) provide sequences of prototypical morphologies, which are sufficient for our purpose of establishing the relation between the degree of phase separation and the performance of polymer solar cells.

B. Exciton generation and diffusion

For each generated morphology, the established four-step mechanism of photocurrent generation (exciton generation, exciton migration, exciton dissociation into an electron-hole pair, and free carrier transport) is simulated to assess the efficiency of the solar cell. We assume that, under a fixed light intensity, the excitons are generated at a constant rate and their transport within the cell occurs through diffusion. In our simulation, the diffusion of excitons is simulated using the random walk model. The jump frequency of the random walk is proportional to the diffusion coefficient D, resulting in an average diffusion distance l that is proportional to the square root of the diffusion time t:

$$l = \sqrt{4Dt}. \tag{4}$$

C. Transport of charge carriers

It is generally accepted that the free carrier transport in polymers follows hopping dynamics, which can be simulated as the hopping of an electron or a hole from one site to another with a rate decided by the energy difference and hopping distance. We adopt the Gaussian disorder model[19] for the distribution of energy states and the Miller–Abraham model[20] for calculating the hopping rates. The hopping rate can be written in the following form:

$$W = W_0 \exp\left(-\frac{\Delta E}{k_B T}\right), \tag{5}$$

where W_0 is a coefficient decided by the carrier mobility and by the distance between the initial and final sites. In the absence of an electric field, ΔE is determined by the energy difference between the initial and the final site; in this case, the carrier transport is dominated by diffusion. The hopping rate can be calculated in a manner similar to the excitonic diffusion considered in the previous section, while the diffusion coefficient can be obtained from the Einstein relation:

$$D = \mu\frac{k_B T}{q}, \tag{6}$$

where μ is the carrier mobility and q is the charge of an electron. In the presence of an electric field, which can be introduced by a work function difference between the electrodes and/or by an external bias, the energy change also depends on the field and is given by

$$\Delta E = U_2 - U_1 - q\mathcal{E}d, \tag{7}$$

where U_1 and U_2 are the initial potential energies of sites 1 and 2, $\mathcal{E}$ is the electric field from site 1 to site 2, d is the hopping distance, and q is the carrier charge, which is positive for holes and negative for electrons.

The bimolecular recombination rate of electrons and holes is given by the following relation:[21]

TABLE I. Experimental setting for simulation.

Parameter	Value	Unit
Exciton generation rate	4×10^{27}	$m^{-3}\ s^{-1}$
Exciton lifetime	0.5	ns
Exciton diffusion length	10	nm
Carrier mobility	0.001	$cm^2\ s^{-1}\ V^{-1}$
Work function of ITO/PEDOT	−5.1	eV
Work function of Ca	−2.9	eV
HOMO of P3HT	−4.9	eV
LUMO of P3HT	−3.0	eV
HOMO of PCBM	−6.3	eV
LUMO of PCBM	−3.7	eV

$$R = \gamma(np - n_{\text{int}}p_{\text{int}}), \tag{8}$$

where n and p are the total carrier concentrations, n_{int} and p_{int} are the intrinsic carrier concentrations, and γ is a constant determined by the mobilities of electrons and holes. The intrinsic carriers are neglected here because their concentration is small in comparison with the concentration of photogenerated carriers. At every step of the Monte Carlo simulation, each electron is assigned a probability for recombination that is proportional to the number of holes. Therefore, the overall recombination rate is proportional to the product of n and p.

A kinetic Monte Carlo approach is used to simulate the movement of electrons and holes in the active layer. At each time step, a random move is attempted for each carrier, and the probability of accepting this move is decided by the change in the carrier energy according to Eq. (5). The photocurrent is calculated from the extraction rate of holes and electrons at the electrodes.

D. Model parameters

In the morphology generation, we set J/k_B, the nearest-neighbor interaction in the Ising model, to 1. The value of J is strongly material dependent and accurate data are difficult to obtain. As discussed in Sec. II A, the morphological evolution in our study depends only on the number of Monte Carlo steps and is insensitive to the numerical value of this parameter.

In our simulations of carrier transport, we used typical experimental data for the poly(3-hexylthiophene)/[6,6]-phenyl-C61-butyric acid methyl ester (P3HT/PCBM) system. Indium in oxide (ITO) is used for anode and calcium is used for cathode. The rate of exciton generation is based on 100 mW light injection, and the device thickness is set to 100 nm. Input data for our simulations are listed in Table I.

In both morphology generation and charge transport situations, each grid point in the 2D map stands for 1 nm, which means that each site has the statistical properties over a region with side length of 1 nm. The length scale of several nanometers will be enough for characterizing nanoscale phase separation, as suggested by typical transmission electron microscopy (TEM) or scanning electron microscopy images.

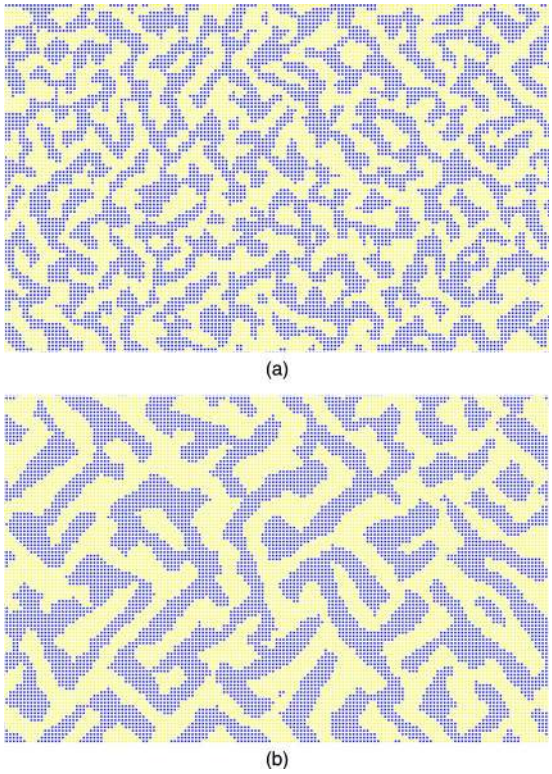

FIG. 1. (Color online) Typical simulation results for morphology generation, showing the influence of annealing time: (a) 10^8 Monte Carlo steps; (b) 10^9 Monte Carlo steps.

III. RESULTS AND DISCUSSION

A. Phase separation

Figure 1 shows the effect of annealing conditions on the morphology due to different annealing times, as measured by the number of Monte Carlo steps. Comparison of Figs. 1(a) and 1(b) shows that increasing the annealing time leads to more phase-separated morphologies. The degree of phase separation can be measured quantitatively using the total entropy of the Ising model and the interfacial area between the phases (or the interface length in two dimensions). The interface length is measured by simply adding up the side lengths of cell borders where different phases lie on two sides. Due to the assumptions of our model, the total entropy correlates very well with the total length of the interface. Figure 2 shows the relation between the area and entropy, exhibiting a highly linear behavior.

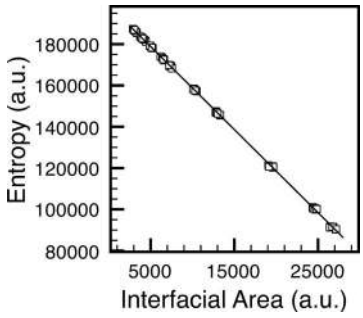

FIG. 2. Relation between the Ising model entropy and the interfacial area.

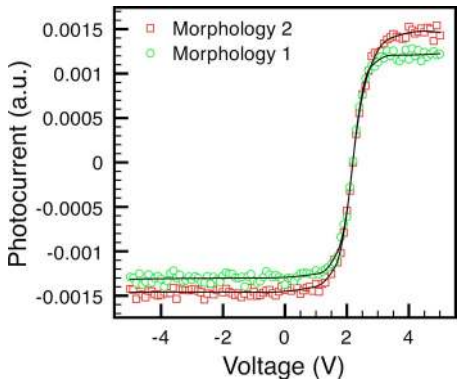

FIG. 3. (Color online) Simulated photocurrent curves for solar cells with different morphologies.

B. Carrier transport

We have compared the carrier transport behavior for all generated morphologies. Figure 3 shows *I-V* curves for two typical samples with different morphologies. Since we did not consider the dark current, i.e., the injection of holes and electrons from the circuit, the current saturates because of the limit on the exciton generation. The two curves in Fig. 3 correspond to simulations on two cells with different morphologies. Obviously, the one with the larger current (morphology 2) is more desired.

Figure 4 shows the dependence of the short circuit current on the interfacial area for all our generated morphologies. There is a clear trend of an optimal range for the interfacial area, which produces the highest photovoltaic current. Below the optimal range, we have systems with smaller interfacial area (higher degree of phase separation) where the rate of the electron-hole pair generation constrains the current. Above the optimal range lie systems with too much interface, which are limited by inefficient conducting paths and high electron-hole recombination rates.[9] The error bars in Fig. 4 give the standard deviations of the current and interfacial area for different runs with the same number of Monte Carlo steps. The scatter in the simulated photocurrent values is due to finite-size effects and morphological information that is not contained in the interfacial area, i.e., with the same degree of phase separation, two solar cells may have different behaviors depending on the higher-order details of phase distribution in the finite area between the electrodes.

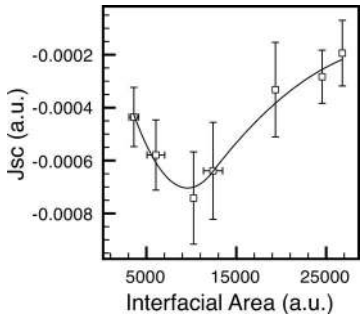

FIG. 4. Relation between the short circuit current and the interfacial area.

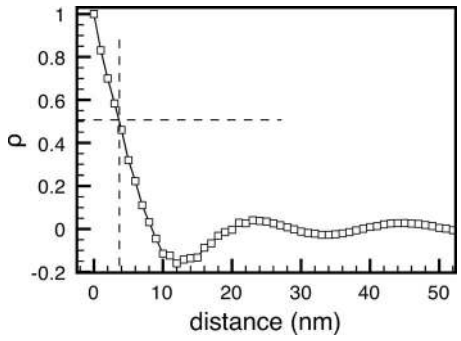

FIG. 5. Correlation function of a sample morphology.

C. Correlation distance

Results of the preceding section show that the interfacial area can be used to characterize the efficiency of solar cells. However, the interfacial area is not a convenient parameter to adopt in practice since it is difficult to measure using microscopy, especially for a three-dimensional system. Here we introduce a simple scalar function that can be easily calculated from a 2D image and assess its efficiency for predicting the performance of solar cells.

The correlation distance is obtained from the pair correlation function ρ,[22] which is defined as

$$\rho_{ij} = \frac{\langle s_i s_j \rangle - \langle s_i \rangle \langle s_j \rangle}{\sigma_{s_i} \sigma_{s_j}} = \langle s_i s_j \rangle, \tag{9}$$

where σ_{s_i} is the rms fluctuation of the spin variable s_i. The correlation function ρ_{ij} is a function of the distance between sites i and j, and in practice, it is obtained by averaging the product $s_i\ s_j$ over all pairs separated by a certain distance $|R_i - R_j|$.

Figure 5 shows the correlation function for a sample morphology, which was obtained after 1×10^{10} Monte Carlo steps. It shows that for a phase-separated morphology, the correlation drops as distance increases, exhibiting a relatively long oscillatory tail. Choosing a threshold in the correlation value ($\rho = 0.5$ in Fig. 5), we define a correlation distance ξ, meaning that pairs at distances smaller than this value are strongly correlated. In other words, the correlation distance gives the characteristic average radius of regions with high probabilities of finding molecules of one type.

The correlation distance can be used to correlate the simulated morphologies with TEM images of solar cells. Figure 6 shows TEM images of a solar cell before and after annealing. This solar cell was found to be one of the most highly efficient ones produced in our group.[23] After filtering the low- and high-frequency portions, which are due to nonuniformity of light and due to noise and aliasing,[24] respectively, we can determine the correlation distance using the same definition as in the simulation. The results are 2 nm before annealing and 3 nm after annealing. The latter value is close to the optimal correlation distance from our simulation, as calculated in the next section.

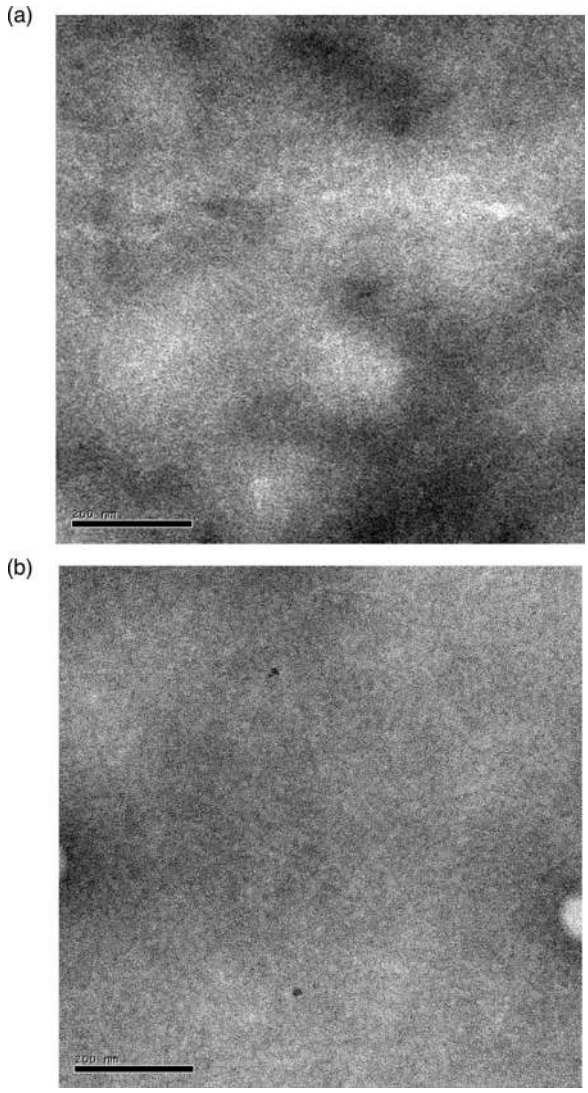

FIG. 6. TEM images of a typical PCBM/P3HT solar cell (a) before and (b) after annealing.

D. Using the correlation distance

The relation between the correlation distance and the interfacial area is shown in Fig. 7. There is an approximate inverse relationship between the two, which implies that, for a 2D system of a given size, the product of these parameters is constant. In other words, the reciprocal correlation distance contains almost the same information as the interfacial area. However, the correlation distance is more useful since (a) the correlation distance can be easily determined from TEM images, while the interfacial area is difficult to measure from microscopy, and (b) the correlation distance is not only a description of the phase boundaries but also a statistical parameter considering both the interface and bulk sites. As shown in Fig. 8, the two morphologies have exactly the same interfacial area, but Fig. 8(a) generates more photocurrent than Fig. 8(b) as a result of a better conduction path. This important difference is well characterized by the correlation distance [4.4 nm in (a) and 9.4 nm in (b)].

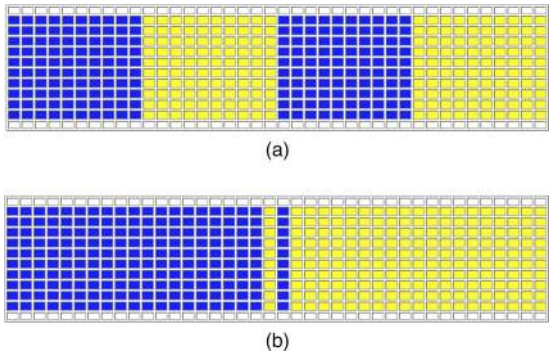

FIG. 8. (Color online) Morphologies with the same interfacial area but different correlation distances.

The correlation distance can also be used to characterize the kinetics of phase separation. Figure 9 shows the Monte Carlo time dependence of the correlation distance. At long times, the rate of increase in ξ follows the relation

$$\xi \propto t^{1/2}, \tag{10}$$

which is consistent with theoretical predictions for the kinetics of phase separation in two dimensions.[25] These results show that by measuring the correlation distance of real systems over time, it should be possible to correlate the degree of phase separation in experiments with our simulation results.

Figure 10 shows the relation between the short circuit current and the correlation distance. This figure tells a story that is similar to the plot of the current versus the interfacial area in Fig. 4, except that we can draw a further quantitative conclusion that in this case the optimal degree of phase separation can be characterized by a correlation distance of approximately 4 nm.

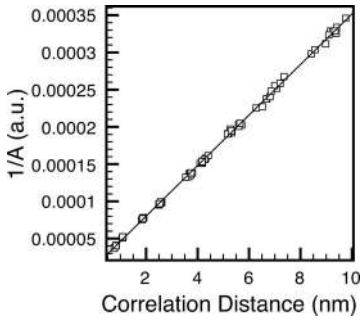

FIG. 7. Relation between the correlation distance and reciprocal interfacial area.

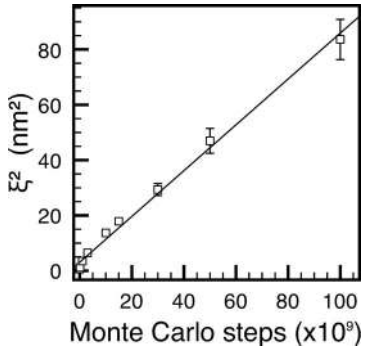

FIG. 9. Correlation distance as a function of the number of Monte Carlo steps.

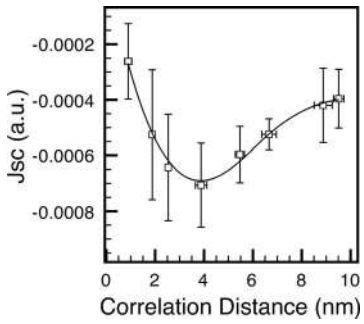

FIG. 10. Short circuit current as a function of the correlation distance. Error bars represent the standard deviations in the simulated morphologies and current values for the same number of Monte Carlo steps.

Figure 11 shows that the short circuit current as a function of the correlation distance strongly depends on the exciton lifetime and diffusion coefficient. Our results demonstrate that longer exciton lifetimes and/or higher exciton diffusion coefficients favor morphologies with longer correlation lengths and higher degrees of phase separation. Other parameters, such as the charge recombination rate and the variance of the energy distribution, are also predicted to have an impact on the relation between the current and correlation distance. Generally, changes in parameters that improve the dissociation of excitons into electrons and holes (e.g., longer exciton lifetimes) will increase the optimal correlation distance, while changes that improve carrier transport (e.g., resulting in lower recombination rates) will favor shorter correlation distances.

IV. CONCLUSIONS

It has been shown that the morphology has a large influence on the short circuit current of a polymer solar cell. An optimal range of phase separation exists due to competition between better electron transport in more phase-separated structures and better rates of exciton creation in less phase-separated ones. The morphology in turn can be controlled by annealing conditions.

We suggest that the correlation distance is a convenient quantity that can be used to accurately characterize the morphology of polymer solar cells. Our simulation results for computer-generated morphologies show that the optimal correlation distance varies with parameters describing the behavior of excitons and charge carriers. Predictions for optimal morphologies in the PCBM/P3HT system are consistent with the values of correlation distances derived from TEM images of optimized solar cells.

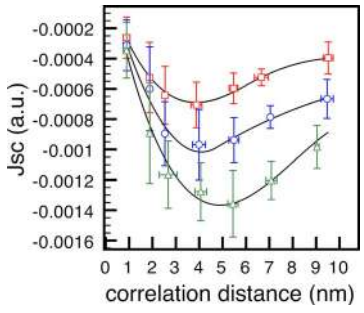

FIG. 11. (Color online) Short circuit current vs correlation distance with different exciton lifetimes. Square, circular, and triangular data points represent exciton lifetimes of 0.5 ns, 1 ns, and 2 ns, respectively.

In the future, more accurate approaches for simulating morphology generation, such as considering the effect of solvent annealing, should be studied. On the other hand, factors other than correlation distance affecting photocurrent generation through various mechanisms should be characterized further, for example, finite-size effects associated with the higher-order details of polymer distribution and ordering in the finite area between the electrodes. Carrying out three-dimensional simulations would also be a promising direction for further improvement.

ACKNOWLEDGMENTS

We would like to thank Dr. Gang Li of Solarmer Energy Inc., El Monte, CA for technical discussion. The financial support for B.L., A.K., and Y.Y. was provided by a grant from Solarmer Energy Inc. and by the Discovery Grant from the University of California. V.O. gratefully acknowledges financial support from the National Science Foundation under Grant No. DMR-0427638.

[1] J. A. Turner, Science **285**, 687 (1999).
[2] S.-S. Sun and N. S. Sariciftci, *Organic Photovoltaics: Mechanisms, Materials, and Devices* (CRC, Boca Raton, 2005).
[3] C. J. Brabec, V. Dyakonov, J. Parisi, and N. S. Sariciftci, *Organic Photovoltaics: Concepts and Realization* (Springer, Berlin, Germany, 2003).
[4] J. Peet, J. Y. Kim, N. E. Coates, W. L. Ma, D. Moses, A. J. Heeger, and G. C. Bazan, Nat. Mater. **6**, 497 (2007).
[5] G. Li, V. Shrotriya, J. Huang, Y. Yao, T. Moriarty, K. Emery, and Y. Yang, Nat. Mater. **4**, 864 (2005).
[6] W. Ma, C. Yang, X. Gong, K. Lee, and A. J. Heeger, Adv. Funct. Mater. **15**, 1617 (2005).
[7] Y. Kim, S. Cook, S. M. Tuladhar, S. A. Choulis, J. Nelson, J. R. Durrant, D. D. C. Bradley, M. Giles, I. McCulloch, C.-S. Ha, and M. Ree, Nat. Mater. **5**, 197 (2006).
[8] G. Yu, J. Gao, J. C. Hummelen, F. Wudl, and A. J. Heeger, Science **15**, 1789 (1995).
[9] P. Watkins, A. Walker, and G. Verschoor, Nano Lett. **5**, 1814 (2005).
[10] R. Janssen, J. Hummelen, and N. Sariciftci, MRS Bull. **30**, 33 (2005).
[11] S. E. Shaheen, C. J. Brabec, F. Padinger, T. Fromherz, J. C. Hummelen, and N. S. Sariciftci, Appl. Phys. Lett. **78**, 841 (2001).
[12] H. Hoppe and N. S. Sariciftci, J. Mater. Chem. **16**, 45 (2006).
[13] D. Chirvase, J. Parisi, J. C. Hummelen, and V. Dyakonov, Nanotechnology **15**, 1317 (2004).
[14] Y. Yao, C. Shi, G. Li, V. Shrotriya, Q. Pei, and Y. Yang, Appl. Phys. Lett. **89**, 153507 (2006).
[15] Y. Yao, Y. Liang, V. Shrotriya, S. Xiao, L. Yu, and Y. Yang, Adv. Mater. (Weinheim, Ger.) **19**, 3979 (2007).
[16] R. Shikler, M. Chiesa, and R. Friend, Macromolecules **39**, 5393 (2006).
[17] K. O. Sylvester-Hvid, S. Rettrup, and M. A. Ratner, J. Phys. Chem. B **108**, 4296 (2004).
[18] P. Peumans, S. Uchida, and S. Forrest, Nature (London) **425**, 158 (2003).
[19] H. Bassler, Phys. Status Solidi B **175**, 15 (1993).
[20] A. Miller and E. Abrahams, Phys. Rev. **120**, 745 (1960).
[21] L. J. A. Koster, V. D. Mihailetchi, and P. W. M. Blom, Appl. Phys. Lett. **88**, 052104 (2006).
[22] W. Feller, *An Introduction to Probability Theory and its Applications* (Wiley, New York, 1968).
[23] G. Li, V. Shrotriya, Y. Yao, and Y. Yang, J. Appl. Phys. **98**, 043704 (2005).
[24] W. Ma, C. Yang, and A. J. Heeger, Adv. Mater. (Weinheim, Ger.) **19**, 1387 (2007).
[25] N. Goldenfeld, *Lectures on Phase Transitions and the Renormalization Group* (Addison-Wesley, Boston, 1996).